Microstructural Investigation of Deformation and Failure Mechanisms in Polypropylene

Antonyraj Arockiasamy*, Esteban Marin, Jean-Luc Bouvard, Paul T. Wang, Mark F. Horstemeyer, Roger L. King and Will Morgan

Center for Advanced Vehicular System, Mississippi State University,
200 Research Boulevard, Starkville, MS 39759, USA

Abstract

The automotive industry continues to expand its use of polymeric materials, which provide more cost effective, strength and durability than metals or ceramics. Thus, a better understanding of the mechanical behavior and microstructural characterization of polymers is essential to develop their improved strength and toughness. This paper describes the deformation and fracture study of commercially available semicrystalline polypropylene (PP). The specimen were subjected to tensile stress using a tensile testing machine and intentionally stopping at three different strain levels (10%, 20%, 35%). Samples were sectioned into different regions and then, using a scanning electron microscope (SEM), studied for microstructural changes, specifically characterization at each extension of the process of crack initiation and propagation. Other techniques, such as x-ray diffraction (XRD) were also employed to determine the crystallinity of the specimen, both on the surface and of the powder collected from the bulk.

Key words: semicrystalline polypropylene, microstructure, tensile test, fracture mechanism

1. Introduction

Due to their strength, toughness, durability, ductility and thermal resistance, polypropylene and its composites are materials of choice for various industrial applications **[1, 2].** However, their fracture behavior varies according to different test conditions. For example, under normal conditions, PP offers good mechanical strength and thermal resistance properties; however, when the operating temperature is set at sub-ambient level, PP shows only moderate fracture performance **[3, 4]**. The primary factors informing fracture performance are molecular weight, the nature of the crystal phase, crystallinity and spherulite size, which in turn vary according to the conditions under which the material was prepared and according to the microstructural morphology. Hence studying factors that are responsible for fracture behavior is essential to develop materials that are resistant to cracking as well as capable of reacting well to stress after initial cracks appear **[5-8].** Numerous papers address the improvement of semicrystalline polymer mechanical behavior **[1-5]**. Copolymerization, the process of blending various additions of elastomers with PP, has significantly improved PP's impact resistance **[9-12].** The elastomers reported to be effective include maleated ethylene-propylene random copolymer (EPR), maleated ethylene-propylene-diene monomer (EPDM), and maleated styrene-ethylene-butylene-styrene block copolymers (SEMB) **[13-15]**.

*Author for correspondence, email aanton@cavs.msstate.edu

Report Documentation Page

Form Approved
OMB No. 0704-0188

1. REPORT DATE	2. REPORT TYPE	3. DATES COVERED
08 FEB 2011	**Journal Article**	**19-06-2010 to 27-10-2010**

4. TITLE AND SUBTITLE
Microstructural Investigation of Deformation and Failure Mechanisms in Polypropylene

5a. CONTRACT NUMBER
w56hzv-08-c-0236

5b. GRANT NUMBER

5c. PROGRAM ELEMENT NUMBER

6. AUTHOR(S)
Antonyraj Arockiasamy; Esteban Marin; Jean-Luc Bouvard; Paul Wang; Mark Horstemeyer

5d. PROJECT NUMBER

5e. TASK NUMBER

5f. WORK UNIT NUMBER

7. PERFORMING ORGANIZATION NAME(S) AND ADDRESS(ES)
Center for Advanced Vehicular System,Mississippi State University,200 Research Boulevard,Starkville,MS,39759

8. PERFORMING ORGANIZATION REPORT NUMBER
; #21511

9. SPONSORING/MONITORING AGENCY NAME(S) AND ADDRESS(ES)
U.S. Army TARDEC, 6501 East Eleven Mile Rd, Warren, Mi, 48397-5000

10. SPONSOR/MONITOR'S ACRONYM(S)
TARDEC

11. SPONSOR/MONITOR'S REPORT NUMBER(S)
#21511

12. DISTRIBUTION/AVAILABILITY STATEMENT
Approved for public release; distribution unlimited

13. SUPPLEMENTARY NOTES

14. ABSTRACT
The automotive industry continues to expand its use of polymeric materials, which provide more cost effective, strength and durability than metals or ceramics. Thus, a better understanding of the mechanical behavior and microstructural characterization of polymers is essential to develop their improved strength and toughness. This paper describes the deformation and fracture study of commercially available semicrystalline polypropylene (PP). The specimen were subjected to tensile stress using a tensile testing machine and intentionally stopping at three different strain levels (10%, 20%, 35%). Samples were sectioned into different regions and then, using a scanning electron microscope (SEM), studied for microstructural changes, specifically characterization at each extension of the process of crack initiation and propagation. Other techniques, such as x-ray diffraction (XRD) were also employed to determine the crystallinity of the specimen, both on the surface and of the powder collected from the bulk.

15. SUBJECT TERMS
semicrystalline polypropylene, microstructure, tensile test, fracture mechanism

16. SECURITY CLASSIFICATION OF:			17. LIMITATION OF ABSTRACT	18. NUMBER OF PAGES	19a. NAME OF RESPONSIBLE PERSON
a. REPORT	b. ABSTRACT	c. THIS PAGE			
unclassified	**unclassified**	**unclassified**	**Public Release**	**19**	

These functionalized polymers copolymerize with PP and establish a strong bond between the phases. In addition, various filling materials, such as glass beads, talc, $CaCO_3$ or reinforcing fibers (short glass fibers, glass), are also being added to improve the stiffness and strength of PP **[13].** Microscopy techniques provide means to evaluate the distribution of such additives and the changes in PP's mechanical behavior which they produce, ultimately to better understand the quality improvement generated via the copolymerization process. **.**

The present work will investigate the factors responsible for fracture behavior in commercially available semicrystalline PP, first examining the sample microstructure at different stages of extension and then correlating the XRD and tension test results to the material/microstructural properties.

2. Materials and experimental details

2.1 Materials

MacMaster supplied the polypropylene (ref. # 2898K) manufactured by Poly Hi Solidur Inc. in sheet form having dimension 12" x 12".

2.2 X-ray diffraction (XRD)

XRD analysis was performed both on the surface and on a powder sample from the bulk of the specimen using CuKα radiation (λ = 0.54 nm). A Rigaku x-ray diffractometer (Ultima III) at a voltage of 40 V and current of 40 mA and a step size of 0.24 deg min^{-1} in a range of 1-50 degree was used. Silicon powder was used as an initial calibration reference.

2.3 Tensile Testing

The samples were subjected to tension test using the Instron 5869 tension testing machine. An axial load was increased at a strain rate of 0.01/s. Each test was intentionally stopped at graduated strain levels: 10%, 20%, and 35%. An untested sample was maintained as a control.

2.4 Scanning Electron Microscopy (SEM)

After tensile testing, the samples were sectioned in different regions and then sputter-coated (magnetron sputter coater, such as the Quorum K550X) with platinum to obtain finer microstructure. A JSM-Jeol 6500A scanning electron microscope was used.

2.5 Image Acquisition

To analyze the polypropylene images, a MATLAB program, developed at the Center for Advanced Vehicular Systems, was used as an image postprocessor. The program requires the

user to identify different properties of the image (e.g., scale number) in μm, smallest area to consider for analysis (in pixels), and the length of the scale bar. Using these values, the program computes the scale in μm/pixel ratio to the image. Each of the images used in this study contained 2558 x 1926 pixels with each pixel represented by a grayscale value in the range of 0 (black) to 255 (white). The areas considered for analysis were 0.001 and 0.0001μm². The program considers all values below the user-inputted threshold values as a pore. The program then takes the selected image and highlights the pores in red. The program can calculate the area, the major axis length, the orientation of each pore, the first neighbor distance, and the minor axis length.

3. Results and Discussion

3.1 XRD measurement

Figure 1 shows the XRD patterns of semicrystalline PP obtained from the surface and from the powder collected in different regions of the bulk. The diffraction patterns from the bulk show promising sharp crystalline peaks with hkl values of 110, 040, 130, 111, and 060 that are absent from the surface analysis. This result reveals that the outer surface was totally composed of amorphous phases, whereas the inner region was made up of mostly crystalline phases. The crystal growth was restricted to near the surface because of localized defects, including chain ends and high chain mobility. Using the MDI Jade 8.0 software to estimate crystallinity from the peak integration, the value was recorded as approximately 95%. A scanning electron micrograph was taken at the defects region (**Figure 2**), which occurred at depths of up to several micrometers from the surface. The crystalline phases appear like thin plates stacked one above the other and are separated by a layer of amorphous materials. This arrangement allows the polymer chains to easily slide over each other which, in turn, changes the properties of brittleness, toughness, stiffness or modulus, optical clarity, creep or cold flow, shear strength, barrier resistance, and long term stability. Consequently, the arrangement of these crystalline phases (parallel or perpendicular to the applied stress) completely controls the fracture behavior..

3.2 Tensile test

Figure 3 shows the tensile test results of PP stressed at different elongation levels. The specimen appearance after tensile testing and where the cuts were made for microstructural investigations are shown in **Figure 4**.

3.2.1 Stress-strain relationship

In general, when an external force is applied to polymeric materials, it first deforms elastically or visco-elastically. When the load is removed, the elastic and visco-elastic deformations completely and spontaneously disappear. However, if the force exceeds a certain threshold, permanent (irreversible) deformation occurs. When a critical stress extends beyond the fracture

level, the sample breaks. **Figure 3** illustrates PP's stages of deformation (from points a through d) during tension testing. Three main changes occurred: neck formation, cold drawing, and strain hardening during the elongation up to several times the original length. Both morphological defects as well as crystalline and amorphous phases mainly controlled these changes. Early in the test, the specimen experienced typical elastic deformation and then returned to its original form upon load- release. Specifically, at the yield point, the strain changed from elastic to plastic.

According to the graph in **Figure 3**, as the load continues to increase, necking occurs at the location where the polymer absorbs energy, i.e., where the stress is concentrated. As extension increases past the yield point, the load appears to decrease. Notably, once necking begins, the geometry of the sample continues to change, which affects the values for the load. Although the sample continues extending, the load values are skewed because the cross-sectional area of the sample gets smaller. After the cold drawing region, the load value starts to increase again. Strain hardening is experienced at these values until fracture. The PP samples were not tested until failure; rather, the tests were stopped at 35% strain. In this study, necking was observed in the specimen at 20% and 35% strain as shown in **Figure 4.** In order to study the morphological changes between samples, and within regions of each sample, the samples were cut and prepared for microscopy investigation.

3.3. Fracture mechanism of PP

The primary factors that determine the fracture mechanism or failure mode of semi-crystalline PP are surface morphological defects, orientation of the crystalline phases, and distribution of amorphous phases.

3.3.1. Effect of morphological defects

There are many factors responsible for the initiation of morphological defects in semi-crystalline PP or very high degree crystalline polymers: *interspherulitic defects*—a weak interface; *interlamellar defects*—absence of amorphous phase in between crystalline lamellae, i.e., a lack of tie molecules ; and *intralamellar defects*—morphological defects such as low molecular weight fraction, chain ends, and chain branching. These factors can contribute to the initiation of brittle fracture. **Figure 5 (a)** and **(b)** illustrate the existence of interspherulitic defects (weak spherulite boundaries) due to a high degree of crystallinity in undeformed sample and transpherilitic cracks generated during tensile deformation.

3.3.2. Effects of Crystalline Phase Distribution

Because the PP contains ~95% crystallinity, the orientation of crystalline phases in the spherulite (spherical semi-crystalline regions inside the polymers) greatly influences the deformation of semi-crystalline PP. As illustrated in **Figure 6**, there are three possible arrangements of crystalline phases with respect to the direction of the applied strain: (a) lamellae running parallel

to the direction of strain, (b) some lamellae tilted, and (c) other lamellae aligned perpendicular to the applied load. According to the crystalline phase arrangement, the structure may possibly be deformed in the following ways when PP is elongated: (a) interlamellar slip (pole regions, **Fig. 6(a)**); (b) lamellar rotation (intermediate regions, **Fig. 6(b)**); and (c) lamellar separation (equatorial regions, **Fig. 6(c)**). At the initial stage of deformation, these processes are mainly controlled by the amorphous phase. As the deformation proceeds, the crystalline regions also undergo dramatic changes.

Figure 7 shows the morphology of PP deformed at different elongation levels and the resulting crack propagation direction in crystalline regions. Based on electron microscopic investigations **(in Figure 7)**, as the lamellae break into mosaic blocks, they may tilt, unfold (destruction of crystalline order), or reorganize into a highly oriented fibrillar structure **[16-18].**

3.3.3. Plastic deformation of spherulites

The plastic deformation of spherulites is linked with ductile behavior. The distortion of spherulites while elongation increases in the direction of the stress involves microvoid formation that is interconnected with pronounced stress whitening. **Figure 9** shows the region where the deformation of spherulites involves microvoids. Here, the intensity of the microvoiding depends strongly on the orientation of the spherulite with respect to the direction of the applied strain. Also, as seen in **Figure 9**, microvoid concentration localized most prominently in the central region where necking occurred.

3.3.4. Effect of amorphous phase

Plastic deformation was observed when the stretching level of PP was low, which is primarily governed by the amorphous phase. **Figure 10(a)**, **(b)**, and **(c)** show the presence of craze, ductile, and brittle behavior on PP, sectioned in different regions. Craze-like phenomena were observed during plastic deformation. Meanwhile, brittle fracture is associated with the polymer's lack of chain mobility which prevents plastic deformation. Neck formation at the critical elongation level is usually associated with ductile fracture. Plastic deformation is preceded until strain hardening due to ongoing molecular orientation, along with drastic changes in the semicrystalline structures, which leads to a significant increase in the mechanical stress. This includes the destruction and/or reorganization of the lamellar (crystalline) phase and the orientation of the interlamellar (amorphous) phase.

As in conventional crazes, in this case there is a coexistence of microscopic voids and tiny fibrils that bridge the craze. However, the craze formation and propagation are geometrically limited by the presence of the crystalline lamellae. In other words, the crazing phenomena are controlled by the actual nanostructure and are highly localized but homogeneously distributed over a large sample volume. **Figure 11** illustrates the process of lamellar separation, microvoid formation, and fibrillation. The high strain sample is dominated by the amorphous phase. As seen in previous samples, the high strain sample pictured in **Figure 12** experienced greater deformations

in the center region than the outside regions. The lateral contraction experienced during this stage of plastic deformation corresponds to the destruction of the remaining crystallites and creates a completely distorted morphology. The microfibrils magnified in **Figures 11 and 12** characterize the amorphous microstructure.

4. Conclusions

The deformation and fracture characteristics of PP have been studied using polymer microscopic techniques. In the semicrystalline polymer, the amorphous and crystalline phases, along with common surface morphological defects, are the most significant factors for determining initiation of fracture. Based on the morphological features observed during an SEM examination of the fracture surface at different extension levels, it is possible to characterize and identify the failure mode of fracture. A road map for the factors responsible for failure, including the location of the crack origin, the mode of crack initiation, the mechanism of crack extension, and the nature of the stress that precipitated the failure, was established in this investigation.

The primary factors in determining the fracture mechanism of semicrystalline PP are the following: a) surface morphological defects, b) orientation of the crystalline phases, and c) amorphous phases. Brittle fracture is more favorable at low elongations, which is primarily governed by the amorphous phase, and ductile fracture is predominant at high elongations, which is governed by the crystalline phases. Both semicrystalline PP and very high degree crystalline polymers demonstrated defective surface-level morphological features, such as interspherulitic defects (a weak interface), interlamellar defects (a lack of tie molecules or the absence of the amorphous phase in between crystalline lamellae), and intralamellar defects (low molecular weight fraction, chain ends, and chain branching). These factors lead to a premature failure due to brittle fracture. In addition to surface defects, the orientations of crystalline phases greatly influence the deformation of semicrystalline PP. Due to interlamellar slip, lamellar rotation, and lamellar separation, the crystal structure reshapes itself parallel to the stress when axially loaded under tension. The plastic deformation of spherical spherulites is linked with ductile behavior. The distortion of spherulites increases microvoid formation that is interconnected with pronounced stress whitening. The rearrangement of the phases allows ductility in deformation, which adds to the mechanical strength of the material. This includes the destruction and/or reorganization of the lamellar (crystalline) phase and the orientation of the interlamellar (amorphous) phase.

Plastic deformation in PP is primarily governed by the amorphous phase. A material lacking chain mobility is prevented from undergoing plastic deformation. Craze-like formations were observed in the samples. As in conventional crazes, a coexistence of micro-voids and fibrillar bridges exist in the samples. However, the craze development and propagation are geometrically restricted by the crystalline lamellae.

Acknowledgements

The authors would like to acknowledge the support of the Center for Advanced Vehicular Systems (CAVS) at Mississippi State University (MSU) and TARDEC.

References

1. Agrawal CM, Pearsall GW, (1991) J Mater Sci 26:1919-1930.
2. Schultz JM, Polymer Eng Sci (1984) 24:770-785.
3. Broberg KB, (1968) Int J Fracture 4:11.
4. K. B. Broberg, J. Mech. Phy. Sol. 23 (1975) 215
5. Spence JCH, (2003) High-Resolution electron microscopy. 3rd ed. Oxford: Oxford University Press.
6. Hirsch PB, (1999) Topics in electron diffraction and microscopy of materials. Boca Raton (FL): CRC Press.
7. Suarez JCM, Coutinho FMB, Sydenstricker TH, (2003) Polymer Testing 22:819-824.
8. Long Y, Shanks RA, (1996) J Appl Polym Sci 62:639-644
9. Ward IM, Hadley DW, (2004) An introduction to the mechanical properties of solid polymers. 2nd ed. Hoboken(NJ): John Wiley & Sons.
10. Bassett DC (2005) Michler GH, Balta-Calleja FJ, editors. Mechanical properties of polymers based on nanostructure and morphology. Boca Raton(FL): CRC Press/Taylor & Francis: 3.
11. Grubb DT, Basset DC (1982) Developments in Crystalline Polymers–I. London: Applied Science.
12. Wunderlich B, (1973) Macromolecular physics: Vol. 1: Crystal structure, morphology, defects; Vol. 2: Crystal nucleation, growth, annealing. New York: Academic Press.
13. Martuscelli E, (1995) Polypropylene: structure, blends, and composites", Vol. 2, edited by J. Krager-Kocsis (Chapman & Hall, London, 1995) ch. 1: 1-24
14. Galli P, Haylock JC, Simonazzi T. (1995) Polypropylene: structure, blends, and composites", Vol. 2, edited by J. Krager-Kocsis (Chapman & Hall, London, 1995) ch. 4: 95-140
15. Pukanszky B, (1995) Polypropylene: structure, blends, and composites, Vol. 3, edited by J. Krager-Kocsis (Chapman & Hall, London, 1995) ch. 1:1-70
16. Kajiyama T, Okada T, Takayanagi M. (1974) J Macromol Sci 39: 1595-1599.
17. Peterlin AJ, (1981) J Macromol Sci Phys B 19:401-405.
18. Krug H, Krabach A, Petermann A (1984) J Polymer 25:1687-1692.

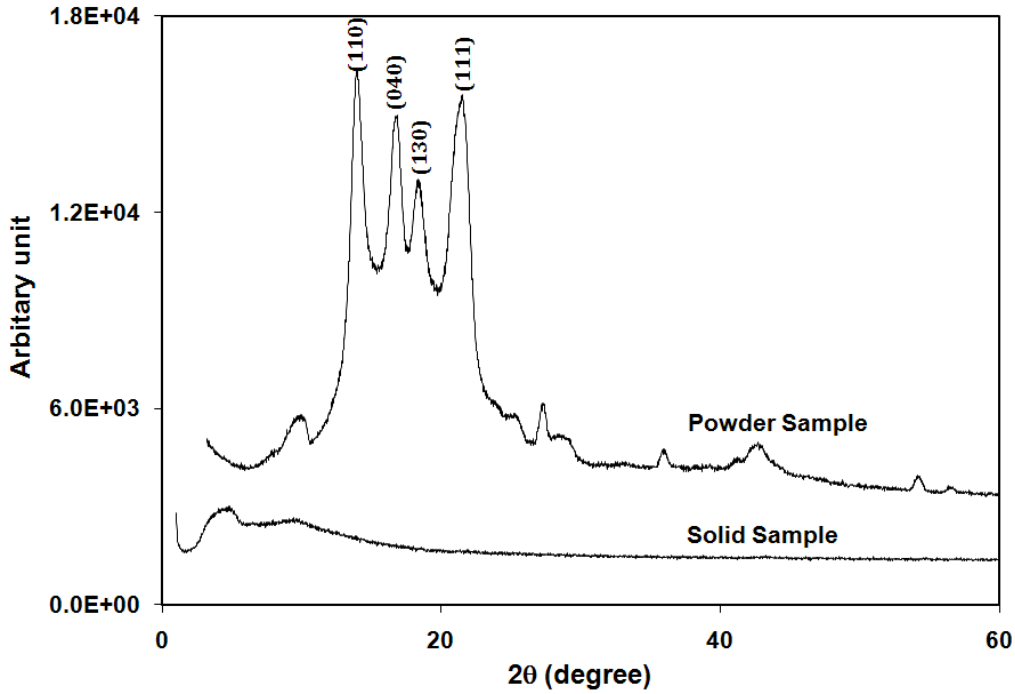

Figure 1 XRD patterns of polypropylene sample surface and powder collected from the bulk showing crystalline peaks.

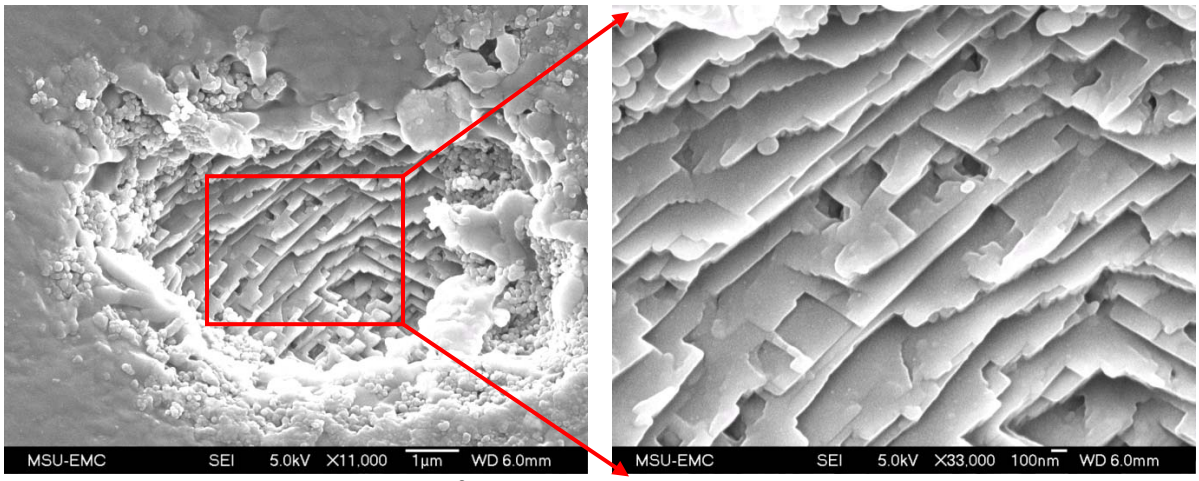

Figure 2 SEM images taken at a defected PP region exploring drastic changes in crystallinity occurring beneath the surface. The second image magnifies the previous image for a magnified look at the structure.

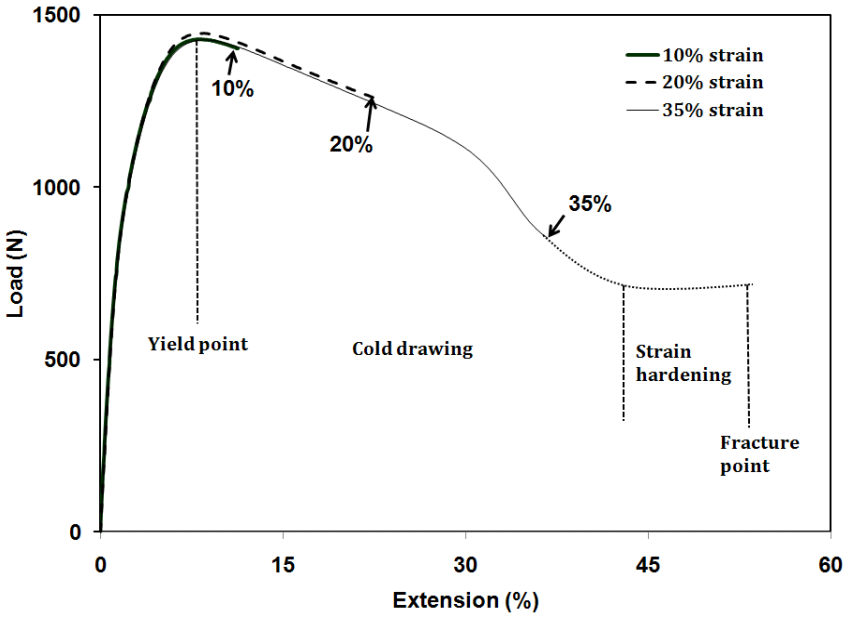

Figure 3 Stress versus strain curves for a commercial polypropylene tested at a strain rate of 0.01/s. Noted are the regions of different stages of deformation such as yield point, cold drawing, strain hardening and fracture.

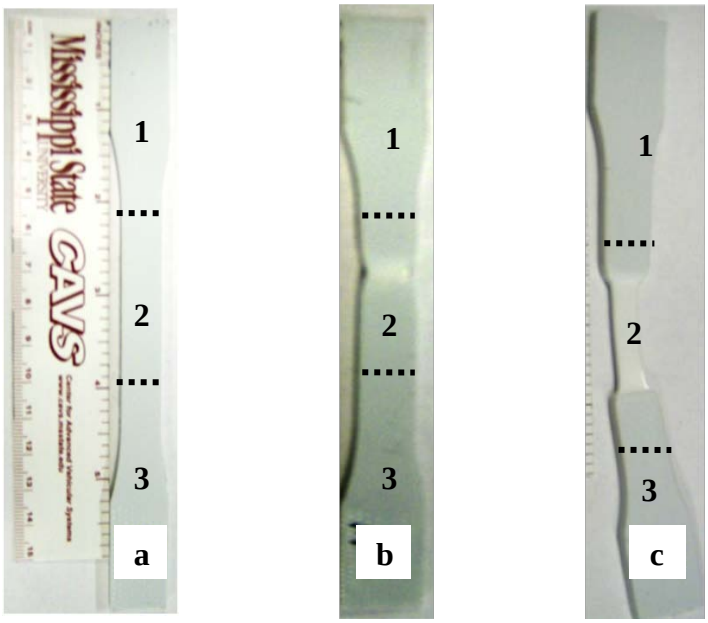

Figure 4 Photographs of PP at different strains (a) 10%, (b) 20%, and (c) 35%. The dotted lines show where cuts were made, dividing each sample into three regions: (1)upper, (2)middle, and (3)lower.

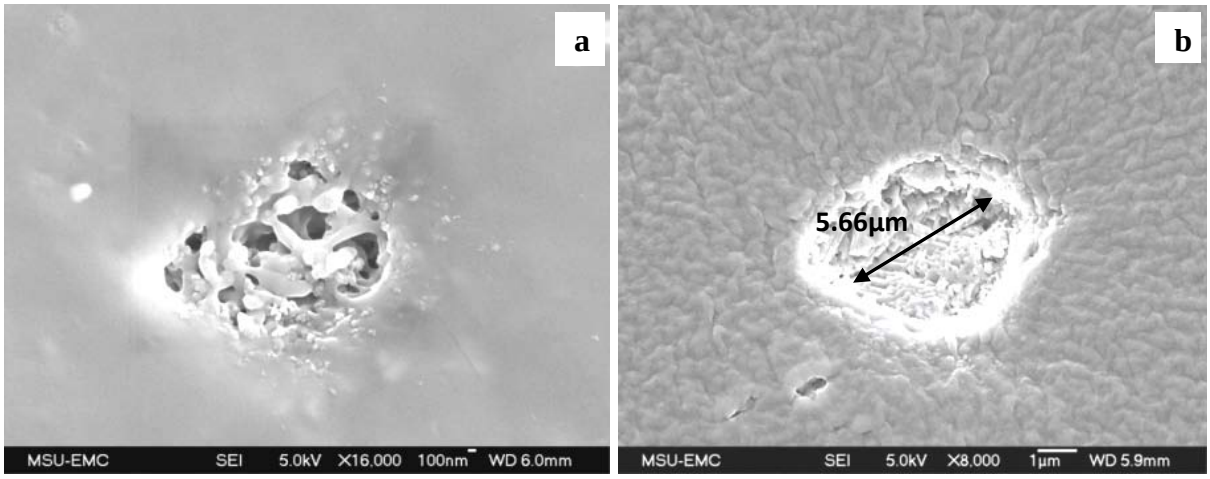

Figure 5 shows the existence of morphological defects in an undeformed sample and tensile tested sample. 5(a) Intersperulitic defects, or weak interface defects, were prevalent for the undeformed sample. This defect is caused by the lack of tie molecules such as amorphous phase between crystalline lamellae. 5(b) Interspherulitic defects (weak spherulite boundaries) due to a high degree of crystallinity is shown in a low strain sample. The distance across the defect was 5.66µm.

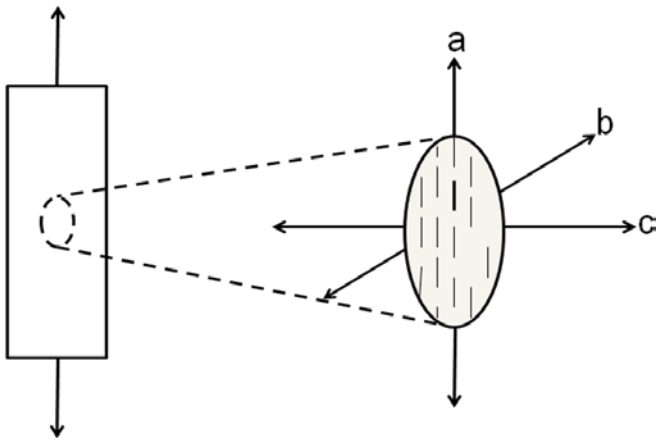

Figure 6 Possible crystalline phase orientations in the spherulite (a) parallel to the direction of strain while (b) some are tilted and (c) others are aligned perpendicular to the applied load.

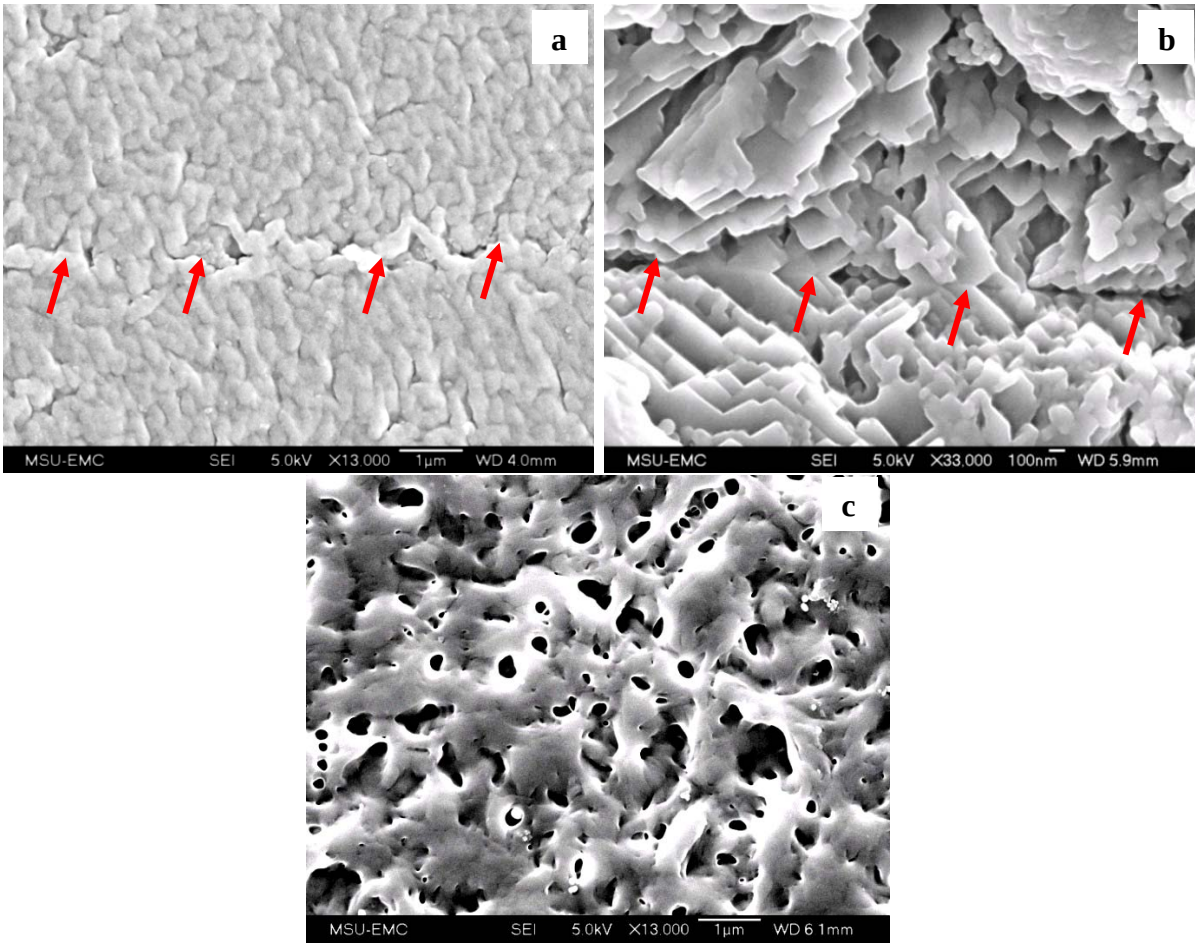

Figure 7 SEM micrographs of semi-crystalline PP deformed at different elongation levels: a) 10%, b) 20%, and c) 35%.

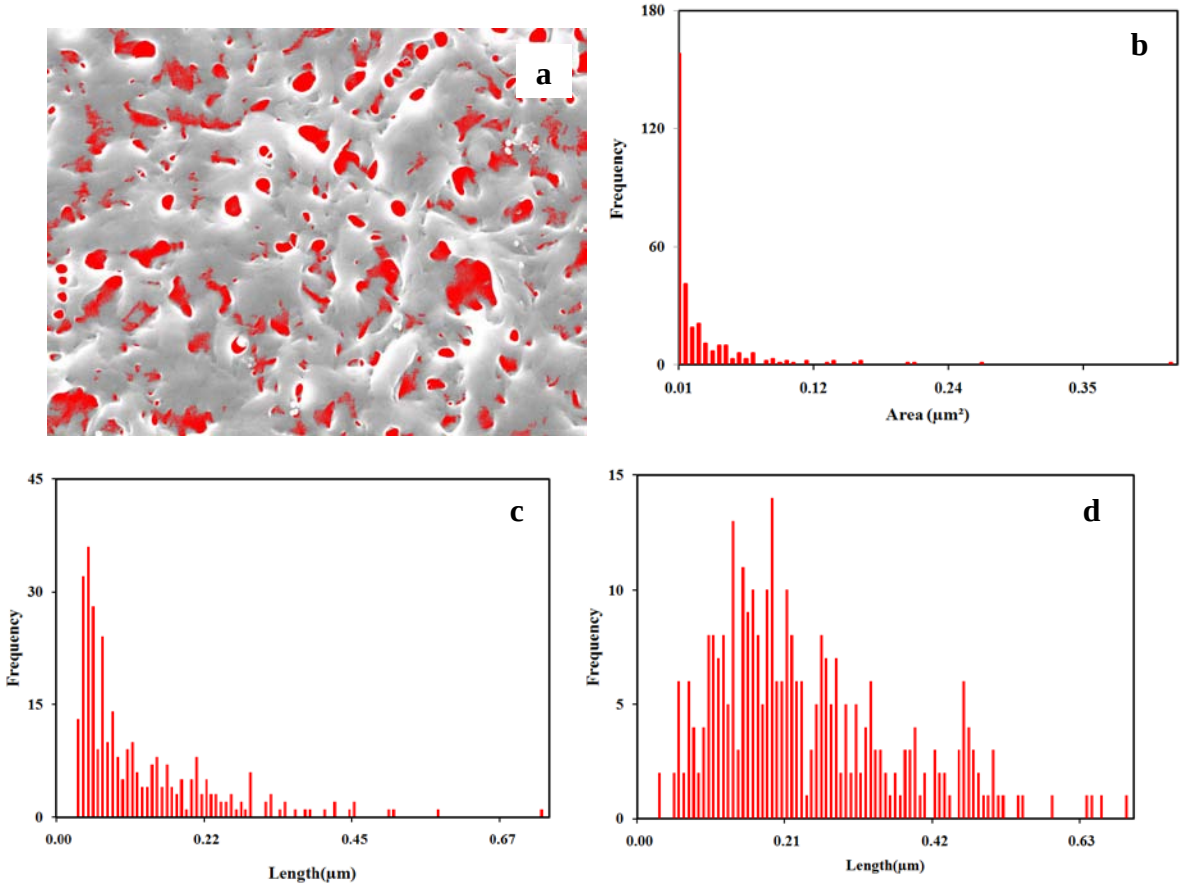

Figure 8 Image with highlighted pores obtained form ImageAnalyzer program (a) freqeuncy to area graph (b), frequency to diameter graph (c), and frequency to nearest neighbor distance (d)

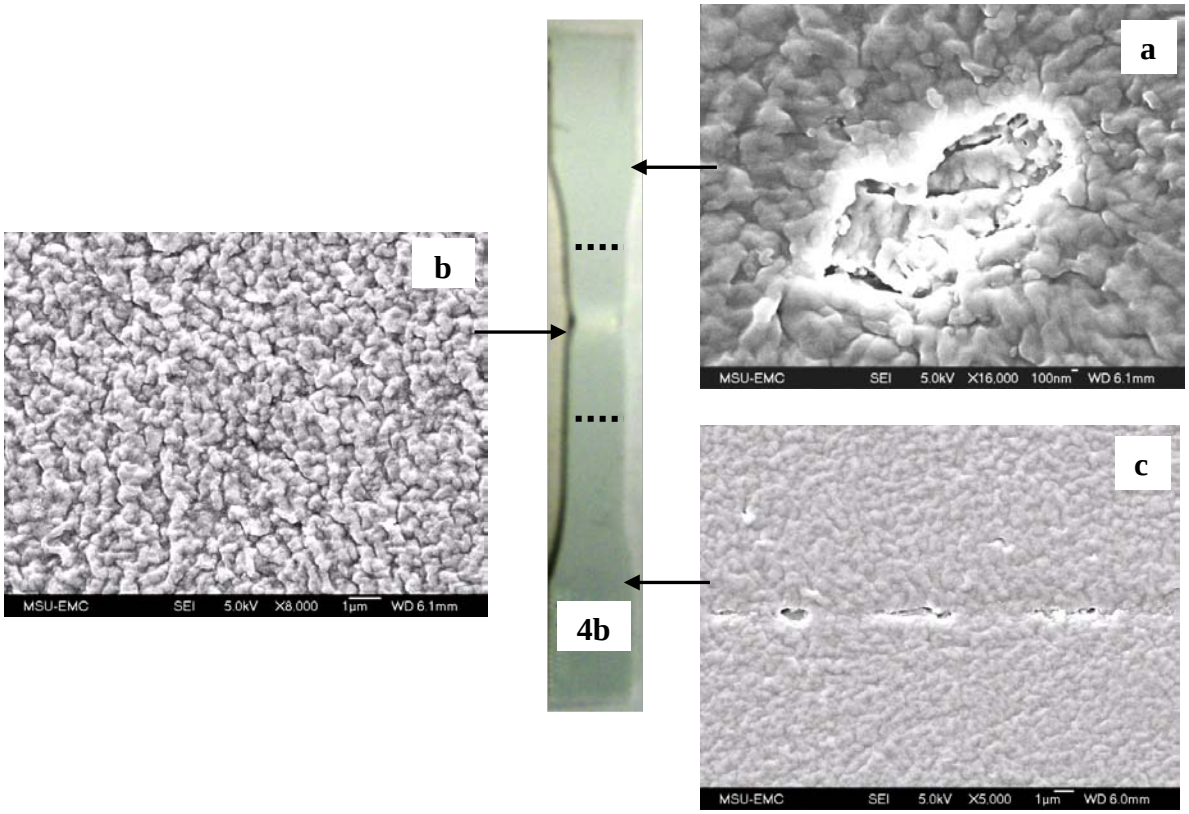

Figure 9 Plastic deformation of spherulites; microvoid formation in spherulites of PP. Images are from a moderately deformed tensile bar exploring the differences between regions. In general, the central region of the sample was more deformed than the outside regions.

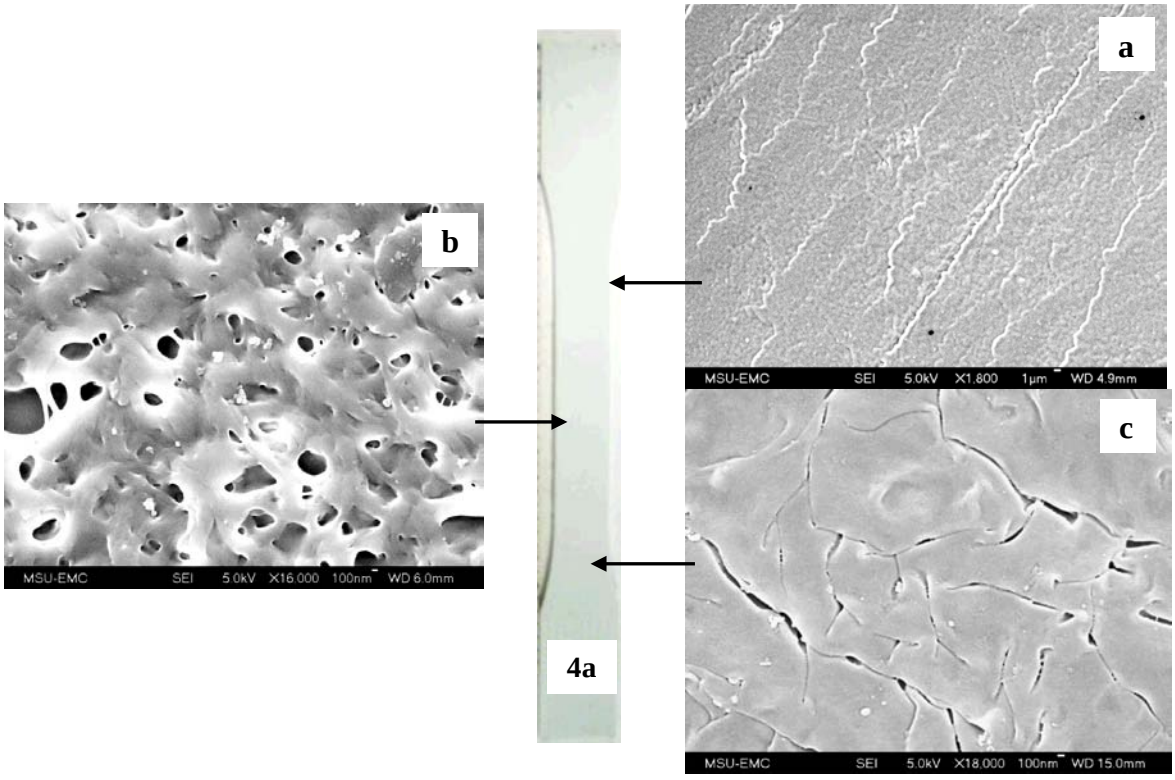

Figure 10 Deformation of semicrystalline PP: a) craze formation, b) ductile behavior, and c) brittle behavior as seen on a low strain sample.

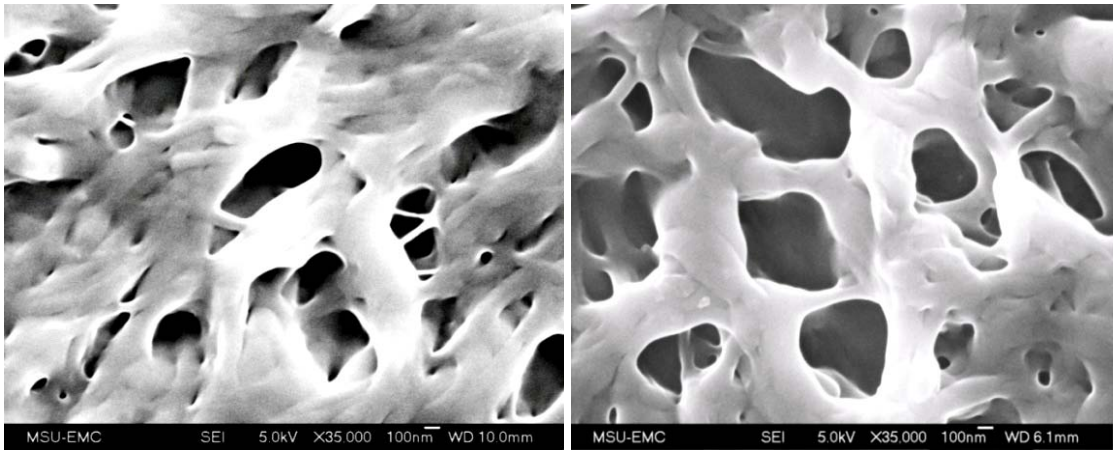

Figure 11 SEM image showing lamellar separation by microvoid formation and fibrillation of the amorphous interlamellar region of deformed PP.

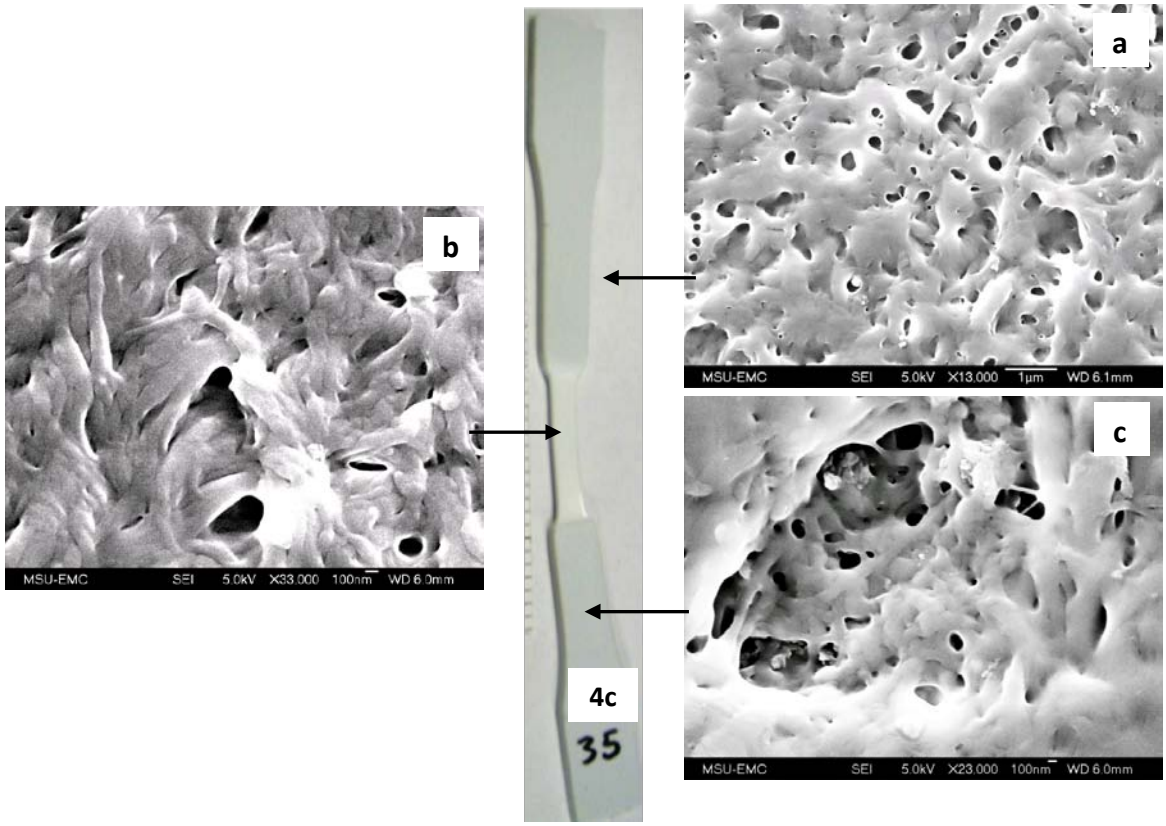

Figure 12 SEM images taken at different regions of the sample. Images were taken on the surface of the sample (a) outside the neck and (b) on the neck. Fig. 12(c) shows a cross-sectional view of the necking region; the image was taken at the cut indicated on the diagram. These images were taken of a deformed specimen at 35% strain.